Nuclear Medicine Communications

Evaluation of delineation of image details in semiconductor PET utilizing the normalized mutual information technique

Naoki Kubo[a], Kenji Hirata[b], Kazuki Matsuzaki[c], Yuichi Morimoto[c], Wataru Takeuchi[c], Naoya Hattori[b], Tohru Shiga[b*], Yuji Kuge[a], Nagara Tamaki[b]

[a]Central Institute of Isotope Science

[b]Department of Nuclear Medicine, Hokkaido University, Sapporo

[c]Central Research Laboratory, Hitachi Ltd, Tokyo, Japan

*Correspondence to Tohru Shiga, PhD, Department of Nuclear Medicine, Hokkaido University, Kita 15 Nishi 7, Kita-ku, Sapporo 060-8638, Japan

Tel: +81 11 706 5152; fax: +81 11 706 7155; e-mail: tshiga@med.hokudai.ac.jp

Objective

PET using semiconductor detectors provides high-quality images of the human brain because of its high spatial resolution. To quantitatively evaluate the delineation of image details in clinical PET images, we used normalized mutual information (NMI) to quantify the similarity with images obtained through MRI. NMI is used to evaluate image quality by determining similarity with a reference image. The aim of this study was to evaluate quantitatively the delineation of image details provided by semiconductor PET.

Materials and methods

To quantitatively evaluate anatomical delineation in clinical PET images, MRI scans of patients were used as T1-weighted images. [^{18}F]-fluorodeoxyglucose (^{18}F-FDG) PET brain images were obtained from six patients using (a) a Hitachi semiconductor PET scanner and a (b) ECAT HR+ scintillator PET scanner. The NMI calculated from the semiconductor PET and MRI was denoted by NMIsemic, whereas the NMI calculated from conventional scintillator PET and MRI was denoted by NMIconve. The higher the value of NMI, the greater the similarity to MRI.

Results

NMIsemic ranged from 1.22 to 1.29, whereas NMIconve ranged from 1.13 to 1.18 (P<0.05). Furthermore, all the NMI values of the semiconductor PET were higher than those of the conventional scintillator PET.

Conclusion

Utilizing NMI, we quantitatively evaluated the delineation of image details in clinical PET images. The results reveal that semiconductor PET has superior anatomical delineation

and physical performance compared with conventional scintillator PET. This improved delineation of image details makes semiconductor PET promising for clinical applications.

Keywords:

image quality; MRI; mutual information; PET; semiconductor

Introduction

PET is a widely applied imaging tool in neuroscience and, over the years, has been accumulating several lines of evidence on the physiological and pathological aspects of brain functions. Also, [^{18}F]-fluorodeoxyglucose (^{18}F-FDG) PET studies have proven useful in the detection of epileptic foci, tumor, and signs associated with a diagnosis of dementia, as well as in differentiating between recurrent tumor and radiation necrosis. However, because of the lower spatial resolution compared with MRI [1], PET images are significantly sensitive to partial volume effect and therefore PET cannot clearly distinguish gray matter, white matter, and cerebrospinal fluid (CSF) in the brain. Furthermore, metabolic change in small structures can be hardly detected with PET.

Semiconductor detectors have in recent times emerged as a new technology in nuclear medicine imaging [2,3]. Flexibility in both sizing and fine arrangement of detectors has improved the spatial resolution and image quality. We have already reported that semiconductor PET provides high-quality images in humans because of its higher spatial resolution [4,5] and have provided useful information for radiation therapy planning [6,7]. However, to demonstrate the usefulness of the higher spatial-resolution semiconductor PET in patient brain imaging, a quantitative measurement of image quality is needed.

To evaluate quantitatively the delineation of image details in clinical PET images, we used a normalized mutual information (NMI) technique to quantify the similarity to individual MRI. NMI is a well-known concept that is often used to image coregistration for both intramodality and intermodality images [8–10]. Recently, Jiang and colleagues [11,12] introduced the use of NMI as a reference image with which to evaluate image quality. We assumed that the NMI-based technique would work successfully for three-dimensional (3D) volume images.

The aim of this study was to evaluate quantitatively the delineation of image details provided by a semiconductor PET that were acquired under different reconstruction methods and acquisition conditions.

Materials and methods

Numerical phantom study

To confirm the ability of NMI in evaluating blurring effects, we applied two numerical phantoms: a cylindrical phantom and a brain-shaped phantom.

Cylindrical phantom

The computer created a single slice consisting of a 256×256 matrix space with each pixel having a floating-point value. The pixel size measured 2 mm^2. Then, the computer generated a cylinder with a diameter of 200 mm, corresponding to the standard size of the adult brain. The in-cylinder pixels had a value of 1.0, whereas the out-of-cylinder pixels had a value of zero. This image was defined as the original image. Blurred images were constructed using 2D Gaussian filters with a full width at half maximum (FWHM) of 9.4, 18.8, 28.3, 37.7, and 47.1 mm. The combination of the original image and each blurred image determined each NMI.

Brain-shaped phantom

The numerical phantom simulating the human brain was produced and published by the Digital Phantom Working Group of Japanese Society of Nuclear Medicine. This phantom contained 128 slices of 128×128 matrixes with each voxel sized 1.75 mm^3. The phantom consisted of three compartments: (a) gray matter with a value of 30.0; (b) white matter with a value of 10.0; and (c) CSF with a value of zero. Out-of-brain tissues such as bone, muscle, fat,

and skin are not considered in this model and take a value of zero. This image was defined as the original. Then, blurred images were constructed using 2D Gaussian filters with an FWHM of 4.7, 9.4, 14.1, 18.8, 23.5, 28.3, 37.7, and 47.1 mm. The combination of the original image and each blurred image determined each NMI.

Semiconductor PET scanner

The specification and the reconstruction algorithm of the semiconductor PET were thoroughly described in our previous paper [4,5]. Briefly, we developed a new PET scanner with cadmium–tellurium semiconductor detectors and a depth-of-interaction (DOI) detection system. The diameter of the patient port is 350 mm, the transaxial field-of-view (FOV) is 310 mm, and the axial FOV is 250 mm. There are 18 detector units radially arranged around the patient port. The new detector size is 2.0×4.0×7.5 mm. The dimensions of the detector unit are 100×400×350 mm. In the unit, the detector boards are arranged in parallel, and the detectors are mounted on both sides of each board. A detector board has 96 detectors on each side (192 detectors in total) and signal processors. These processors include application-specific integrated circuits mounted along the incident direction of γ-rays. Signals are read by a three-layer DOI system. Each unit has 22 boards and about 4000 detectors. The entire system is cooled by forced air. Cadmium–tellurium detectors have a good energy resolution; therefore, the energy window was 490–530 keV. Images were acquired with a 3-min transmission scan using linear source of Cs-137 and then with a 30-min emission scan. Images were reconstructed using the novel algorithm implemented with median root prior and maximization *a posteriori*. The matrix size, pixel size, slice thickness, and diameter of FOV were 256×256, 1.2×1.2 mm, 2.6 mm, and 310 mm, respectively. The spatial resolution at the center of the FOV was 2.3 mm FWHM after reconstruction.

Conventional scintillator PET

The conventional scintillator PET used was ECAT HR+ (Asahi-Siemens Medical Technologies Ltd, Tokyo, Japan). This detector consists of a $Bi_4Ge_3O_{12}$ block. Images were acquired with a 3-min transmission scan (Ge-68 source) and a 10-min emission scan. The images were reconstructed with the brain mode of the manufacturer's software. The energy window was 350–650 keV. The acquired 3D sinograms were converted into 2D sinograms with the Fourier rebinning algorithm. The images were reconstructed using direct-inversion Fourier transformation with a Hanning filter of 4 mm FWHM [13]. The matrix size, pixel size, slice thickness, and diameter of the FOV were 256×256, 1.3×1.3 mm, 2.4 mm, and 330 mm, respectively. The spatial resolution was 6.4 mm FWHM after reconstruction.

Patients study

From September 2008 to March 2009, 30 patients with brain tumor or epilepsy underwent ^{18}F-FDG PET scanning, with the images being acquired using both the semiconductor PET and the conventional scintillator PET on the same day. Out of the 30 patients, we selected six patients on the basis of the following criteria: (a) MRI was performed within an interval of 1 day and (b) the lesion showed lower ^{18}F-FDG uptake than physiological uptake in the normal cortex. Also, we chose the cases with uniform intratumoral distribution in both PET and MRI. Table 1 shows the characteristics of the patients included in this study. The Ethics Committee of the Hokkaido University Hospital approved the study, and all the patients or the parent, if the patient was younger than 20 years of age, gave written informed consent.

Before the PET study all patients fasted for at least 6 h. Following the measurement of serum glucose level confirming normoglycemia in each patient, 349±81 MBq of ^{18}F-FDG was

injected intravenously. Images of the patients were acquired with semiconductor PET and conventional scintillator PET scanners in random order.

MRI scans

MRI scans were obtained with 1.5 T scanners (Magnetome Vision or Magnetome Symphony; Asahi-Siemens Medical Technologies Ltd). Transaxial T1-weighted images without contrast material were acquired as a part of routine examination. All images with a slice thickness of 5 mm without slice gap were reconstructed.

Calculation of normalized mutual information

NMI is an index that represents entropy-based image similarity invariant to the overlapped region of two images [14]. NMI of the combination of 3D volume image A and 3D volume image B is defined as: NMI(A,B) = (H(A) + H(B))/H(A,B), where H(A) and H(B) are the Shannon's entropy of A and B, and H(A,B) is the joint entropy of A and B. The joint probability histogram of the two images (2D histogram) computes H(A), H(B), and H(A,B).

Image coregistration

Images were coregistered on the basis of maximization of NMI. Registration transformations were restricted to the rigid-body type. A nonlinear least square method determined the optimal combination of parameter values. An experienced nuclear physician visually confirmed the successful coregistration in each case. The process was performed using an in-house software based on a previously recommended method [9].

The NMI calculated between semiconductor PET and MRI in 3D was defined as NMIsemic, and the NMI calculated between conventional scintillator PET and MRI in 3D was defined as NMIconve.

Statistical analysis

The Wilcoxon test was performed to determine the significance of difference in NMI between NMIsemic and NMIconve.

Results

Numerical phantom study

Figure 1 summarizes the results of the numerical phantom studies. Figure 1a shows representative images of the cylindrical phantom (top) and the brain phantom (bottom), with their original images allocated to the left and the others being blurred images obtained from Gaussian filters with different FWHM values. In the cylindrical phantom study, the NMI monotonically decreased as the smoothing filter became stronger (Fig. 1b). The NMI had an initial value of 2.00 when a filter of 0 mm FWHM (no blur) was applied, but decreased to 1.53 when 47.1 mm FWHM blurring was applied. In the brain phantom study also NMI monotonously decreased with increasing strength of the smoothing filter. The NMI had an initial value of 2.00 when a filter of 0 mm FWHM (no blur) was applied, but decreased to 34 when 47.1 mm FWHM blurring was applied. Thus we see that the higher the NMI, the better the results.

Patients' images

The clinical study is summarized in Table 1. Figure 2 shows representative images of MRI, semiconductor PET, and conventional scintillator PET. The brain tumor boundary (white arrow) and Sylvian fissure (black arrow) were clearly reproduced in the image of the semiconductor PET. A higher NMI gives better results. NMIsemic ranged from 1.22 to 1.29, and NMIconve ranged from 1.13 to 1.18. Figure 3 shows that NMIsemic was, without exception, higher compared with NMIconve ($P<0.05$).

Discussion

Using numerical values we have demonstrated that the semiconductor PET is superior in terms of delineation of image details under clinical conditions (acquisition time and reconstruction method), as well as in terms of physical performance.

We performed quantitative evaluation of the delineation of image details in clinical PET utilizing the NMI technique. NMI from the semiconductor PET was higher without any exception compared with the NMI from the conventional scintillator PET. Moreover, NMI of the original image and of each blurred image decreased as spatial blur increased in the phantom study.

The semiconductor PET performance

We have already reported that semiconductor PET provides high-quality images of the human head and neck as determined through visual evaluation and the comparison of profile curves.

The semiconductor PET has two well-known advantages [4,5]. First, the photopeak of a semiconductor detector is generally shaper than that of a scintillation detector because of its higher energy resolution [15]. Therefore, semiconductor PET provides high-contrast images with less scatter noise. Second, individual readout is enabled in semiconductor PET with densely packed detectors connected to each amplifier with a one-to-one relationship. This system improves intrinsic spatial resolution compared with a traditional PET detector unit with a positional computer (e.g. Anger-type camera vs. pixelated camera) [16]. Further, our semiconductor PET has two more features that enable high spatial resolution: (a) a smaller detector and (b) a DOI system. A DOI detection system may reduce parallax errors at the periphery of the FOV in PET scanners dedicated to human brain imaging [17]. In fact, the intrinsic spatial resolution of our PET scanner was 2.3 mm at 1 cm or 4.8 mm at 10 cm

from the center of the FOV. This spatial resolution was higher than that of a conventional PET camera and almost similar to that of EXACT HRRT (Siemens Medical Solutions, Knoxville, Tennessee, USA) in a transaxial slice [17].

Use of normalized mutual information

Using the NMI technique, we performed a quantitative comparison of PET images acquired under different reconstruction methods and acquisition conditions.

Image similarity can be evaluated using the least square method as well; however, we did not apply this method in the current study. The least square method considers the pixel value as continuous scalar and thus can be used only when the same structure shows the same pixel value with normalization. Therefore, the use of the least square method is limited to an analysis of intramodality image similarity. In contrast, the NMI concept, derived from information theory, measures the amount of information that one image has about the other [18].

We performed quantitative evaluation of semiconductor PET images using NMI. In the current study, the 2D histogram indicates correspondences between any PET pixel value and the MRI signal. Kruggel and colleagues described that the NMI of the 2D histogram is a general parameter describing image quality: in an ideal image with *n* (any integer) intensity classes without noise, intensity inhomogeneities, partial volume effect, and an ideal point spread function, this joint histogram would consist of *n* peaks. Any deviance from ideal conditions smooths out peaks and decreases the (negative) mutual information. Thus, higher NMI values correspond to similarity with the ideal image [19]. In this study, individual MRIs were used for ideal images. MRIs have high spatial resolution and contrast of soft tissues [1]. We demonstrated that NMIsemic values were higher than NMIconve values, suggesting that

semiconductor PET images have higher similarity compared with scintillator PET images. Therefore, the semiconductor PET is superior to the conventional scintillator PET in anatomical delineation.

NMI describes the dispersive behavior of the 2D histogram [18]. The spatial blur in PET induced 'spill over' from the gray matter. The activity of the specific area in white matter increased, and scatter plots were broad in the 2D histogram. Consequently, NMI values decreased as seen from the dispersive behavior of the 2D histogram.

In this study, we demonstrated that image blurring reduced NMI proportionately to the strength of the filter in both the cylindrical phantom and the brain phantom and that NMIsemic calculated using MRI and semiconductor PET was always higher than NMIconve calculated using MRI and conventional scintillator PET. These results suggest that PET image smoothness can be measured using NMI and that semiconductor PET produced less smooth similar images compared with conventional scintillator PET.

In addition, it was already demonstrated that NMI values calculated between the reference image and acquired images can be used to evaluate image quality [11,12,20].

Patient study

We next investigated the brain images of the patients. Images were coregistrated on the basis of maximization of NMI. An experienced nuclear physician visually confirmed the successful coregistration in each case.

To comparatively evaluate PET images from the two different scanners, we used MRI as reference images, like the no-blur original images used for the phantom study. MRI has a much better spatial resolution than any PET scanner [1]. We assumed that the MRI T1-weighted image and the ^{18}F-FDG PET have specific and homogenous value for gray matter,

white matter, and CSF. We chose uniform intratumoral distributions for both PET and MRI. Furthermore, because of the pathological discrepancy between MRI and PET in terms of lesions, patients who had a lesion with positive ^{18}F-FDG uptake were carefully excluded to minimize the effect of heterogeneity. The PET image with better spatial resolution has similar distribution to MRI and therefore should give higher NMI in combination with MRI. We obtained greater NMI from semiconductor PET than from conventional scintillator PET in all cases. We have previously demonstrated the higher physical performance of semiconductor PET over conventional scintillator PET [4,5], and our current results support this already proven superiority.

Clinical impact

Through improved contrast and spatial resolution, semiconductor PET can contribute tremendously to clinical diagnosis and neuroscience research. Until now, a significant partial volume effect may have caused an underestimation of the metabolism in small structures adjacent to the ventricles, including the hippocampus, basal ganglia, and thalamus [21]. These areas are especially important for the diagnosis of epilepsy and neurodegenerative disorders (Parkinson, corticobasal degeneration, etc.). A smaller partial volume effect can improve the diagnostic performance [22]. We are considering the clinical significance of the semiconductor PET in oncology. Identification of active tumor lesions as a result of the high level of delineation may be valuable in biopsy and radiation planning [5–7].

A limitation of this study is that we did not compare the semiconductor PET with a state-of-the-art PET; rather, we compared it with a relatively old camera, the HR+ system, with direct-inversion Fourier transformation reconstruction. However, the HR+ system provides relatively high-resolution and high-quality PET images with the current

reconstruction algorithm. In the future we consider it necessary to compare a state-of-the-art lutetium oxyorthosilicate PET camera with our semiconductor PET.

Utilizing the NMI technique, we performed quantitative evaluation of the delineation of image details in clinical PET acquired under different reconstruction methods and acquisition conditions. Although it is necessary to compare with state-of-the-art PET systems, the semiconductor PET has been found to be superior to conventional scintillator PET in anatomical delineation as well as in physical performance. Therefore, the semiconductor PET has potential for clinical usefulness because of higher delineation of image details.

Acknowledgements

Conflicts of interest

There are no conflicts of interest.

References

1. Gregoire V, Chiti A. PET in radiotherapy planning: particularly exquisite test or pending and experimental tool?. Radiother Oncol 2010; **96**:275-276.
2. Kubo N, Zhao S, Fujiki Y, Kinda A, Motomura N, Katoh C, *et al.* Evaluating performance of a pixel array semiconductor SPECT system for small animal imaging. Ann Nucl Med 2005; **19**:633-639.
3. Tsuchiya K, Takahashi I, Kawaguchi T, Yokoi K, Morimoto Y, Ishitsu T, *et al.* Basic performance and stability of a CdTe solid-state detector panel. Ann Nucl Med 2010; **24**:301-311.
4. Shiga T, Morimoto Y, Kubo N, Katoh N, Katoh C, Takeuchi W, *et al.* A new PET scanner with semiconductor detectors enables better identification of intratumoral inhomogeneity. J Nucl Med 2009; **50**:148-155.
5. Morimoto Y, Ueno Y, Takeuchi W, Kojima S, Matsuzaki K, Ishitsu T, *et al.* Development of a 3D brain pet scanner using CdTe semiconductor detectors and its first clinical application. IEEE Trans Nucl Sci 2011; **58**:2181-2189.
6. Yasuda K, Onimaru R, Okamoto S, Shiga T, Katoh N, Tsuchiya K, *et al.* [(18)F]fluoromisonidazole and a new PET system with semiconductor detectors and a depth of interaction system for intensity modulated radiation therapy for nasopharyngeal cancer. Int J Radiat Oncol Biol Phys 2013;**85**:142-147.
7. Katoh N, Yasuda K, Shiga T, Hasegawa M, Onimaru R, Shimizu S, *et al.* A new brain positron emission tomography scanner with semiconductor detectors for target volume delineation and radiotherapy treatment planning in patients with nasopharyngeal carcinoma. Int J Radiat Oncol Biol Phys 2012; **82**:e671-e676.
8. Yokoi T, Soma T, Shinohara H, Matsuda H. Accuracy and reproducibility of co-registration techniques based on mutual information and normalized mutual information for MRI and SPECT brain images. Ann Nucl Med 2004; **18**:659-667.
9. Zhu YM, Cochoff SM. Influence of implementation parameters on registration of MR and SPECT brain images by maximization of mutual information. J Nucl Med 2002; **43**:160-166.
10. Wong JC, Studholme C, Hawkes DJ, Maisey MN. Evaluation of the limits of visual detection of image misregistration in a brain fluorine-18 fluorodeoxyglucose PET-MRI study. Eur J Nucl Med 1997; **24**:642-650.
11. Jiang X. Iterative reconstruction method for three-dimensional non-Cartesian parallel MRI [theses and dissertations]. Iowa City: University of Iowa; 2011; pp. 1–128
12. Odille F, Cîndea N, Mandry D, Pasquier C, Vuissoz PA, Felblinger J. Generalized MRI reconstruction including elastic physiological motion and coil sensitivity encoding. Magn

Reson Med 2008; **59**:1401-1411.

13. Stark H, Woods JW, Paul I, Hingorani R. An investigation of computerized tomography by direct Fourier inversion and optimum interpolation. IEEE Trans Biomed Eng 1981; **28**:496-505.
14. Studholme C, Hill D, Hawkes D. An overlap invariant entropy measure of 3D medical image alignment. Pattern Recognit 1999; **32**:71-86.
15. Ueno Y, Morimoto Y, Tsuchiya K, Yanagita N, Kojima S, Ishitsu T, *et al.* Basic performance test of a prototype PET scanner using CdTe semiconductor detectors. IEEE Trans Nucl Sci 2009; **56**:24-28.
16. Kubo N, Mabuchi M, Katoh C, Arai H, Morita K, Tsukamoto E, *et al.* Validation of left ventricular function from gated single photon computed emission tomography by using a scintillator-photodiode camera: a dynamic myocardial phantom study. Nucl Med Commun 2002; **23**:639-643.
17. Schmand M, Eriksson L, Casey M, Andreaco M, Melcher C, Wienhard K, *et al.* Performance results of a new DOI detector block for a high resolution PET-LSO research tomograph HRRT. IEEE Trans Nucl Sci 1998; **45**:3000-3006.
18. Maes F, Collignon A, Vandermeulen D, Marchal G, Suetens P. Multimodality image registration by maximization of mutual information. IEEE Trans Med Imaging 1997; **16**:187-198.
19. Kruggel F, Turner J, Muftuler LT. Impact of scanner hardware and imaging protocol on image quality and compartment volume precision in the ADNI cohort. Neuroimage 2010; **49**:2123-2133.
20. Shao L, Hero AO, Rogers WL, Clinthorne NH. The mutual information criterion for SPECT aperture evaluation and design. IEEE Trans Med Imaging 1989; **8**:322-336.
21. Kalpouzos G, Chételat G, Baron JC, Landeau B, Mevel K, Godeau C, *et al.* Voxel-based mapping of brain gray matter volume and glucose metabolism profiles in normal aging. Neurobiol Aging 2009; **30**:112-124.
22. Kato H, Shimosegawa E, Oku N, Kitagawa K, Kishima H, Saitoh Y, *et al.* MRI-based correction for partial-volume effect improves detectability of intractable epileptogenic foci on ^{123}I-iomazenil brain SPECT images. J Nucl Med 2008; **49**:383-389.

Fig. 1

Results of numerical phantom studies. (a) Representative images of cylindrical phantom (top) and brain phantom (bottom) along with their original images (left) and blurred images generated by Gaussian filters. (b) The normalized mutual information of the cylindrical phantom (open circles) and brain phantom (filled circles) decreases monotonically with increasing filter strength. 2D, two-dimensional; FWHM, full width at half maximum.

Fig. 2

Representative (a) MRI, (b) semiconductor PET, and (c) conventional scintillator PET (case 2) images.

Fig. 3

Normalized mutual information obtained using MRI as reference images for six patients.

Table 1 Patient characteristics

Patient number	Age	Sex	Weight (kg)	Diagnosis	Dosage (MBq)
1	15	F	95	Epilepsy	347
2	74	M	63	Glioma	382
3	60	F	50	Glioma	410
4	36	M	76	Glioma	377
5	40	M	86	Glioma	389
6	4	M	18	Epilepsy	190
Mean±SD	38±26		65±28		349±81

Fig.1

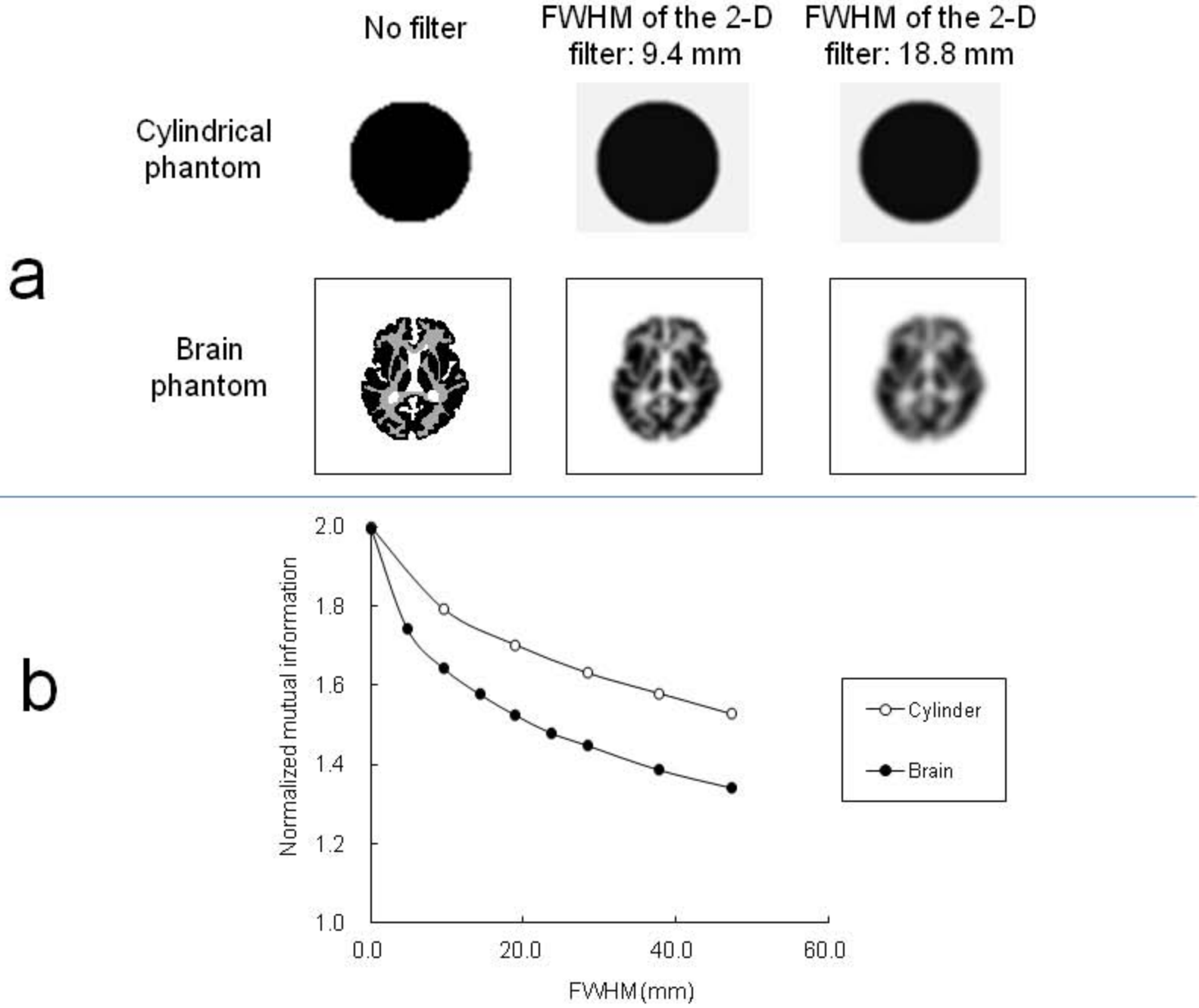
No filter
FWHM of the 2-D filter: 9.4 mm
FWHM of the 2-D filter: 18.8 mm
Cylindrical phantom
a
Brain phantom
b
Normalized mutual information
2.0
1.8
1.6
1.4
1.2
1.0
0.0
20.0
40.0
60.0
FWHM (mm)
Cylinder
Brain

Fig.2

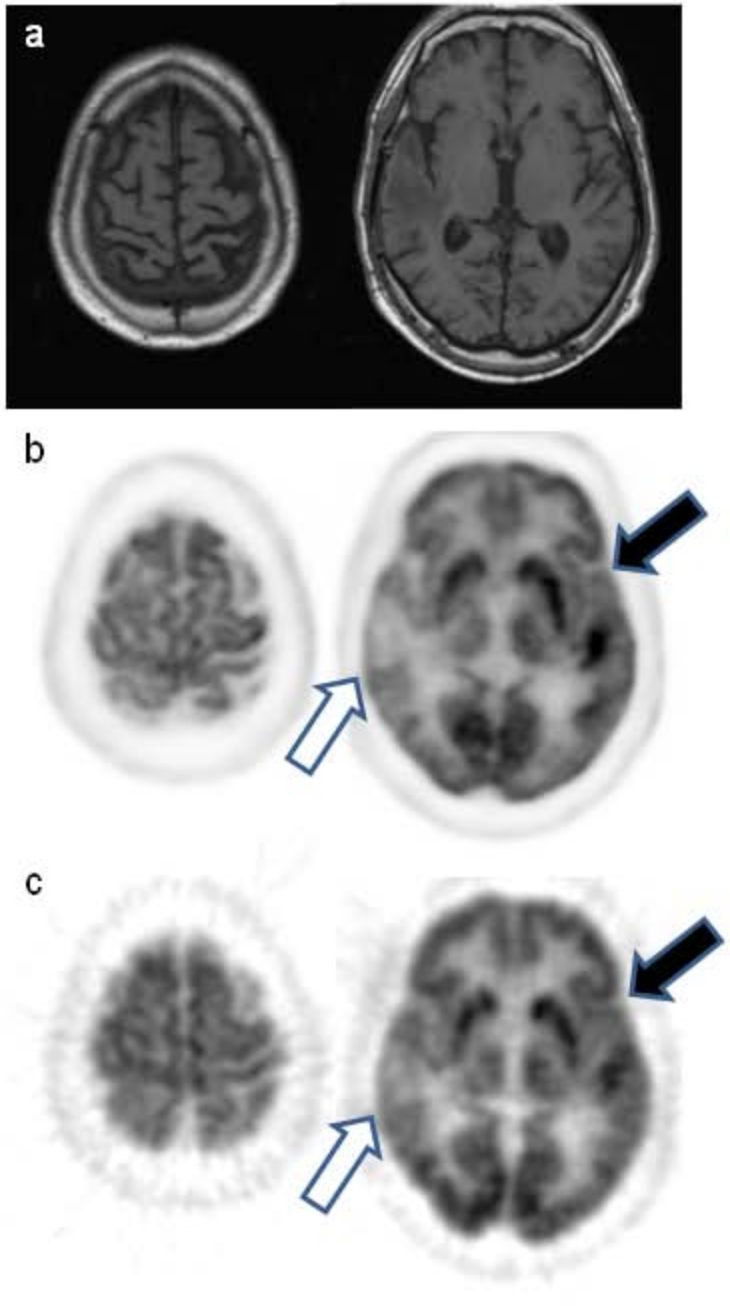

Fig.3

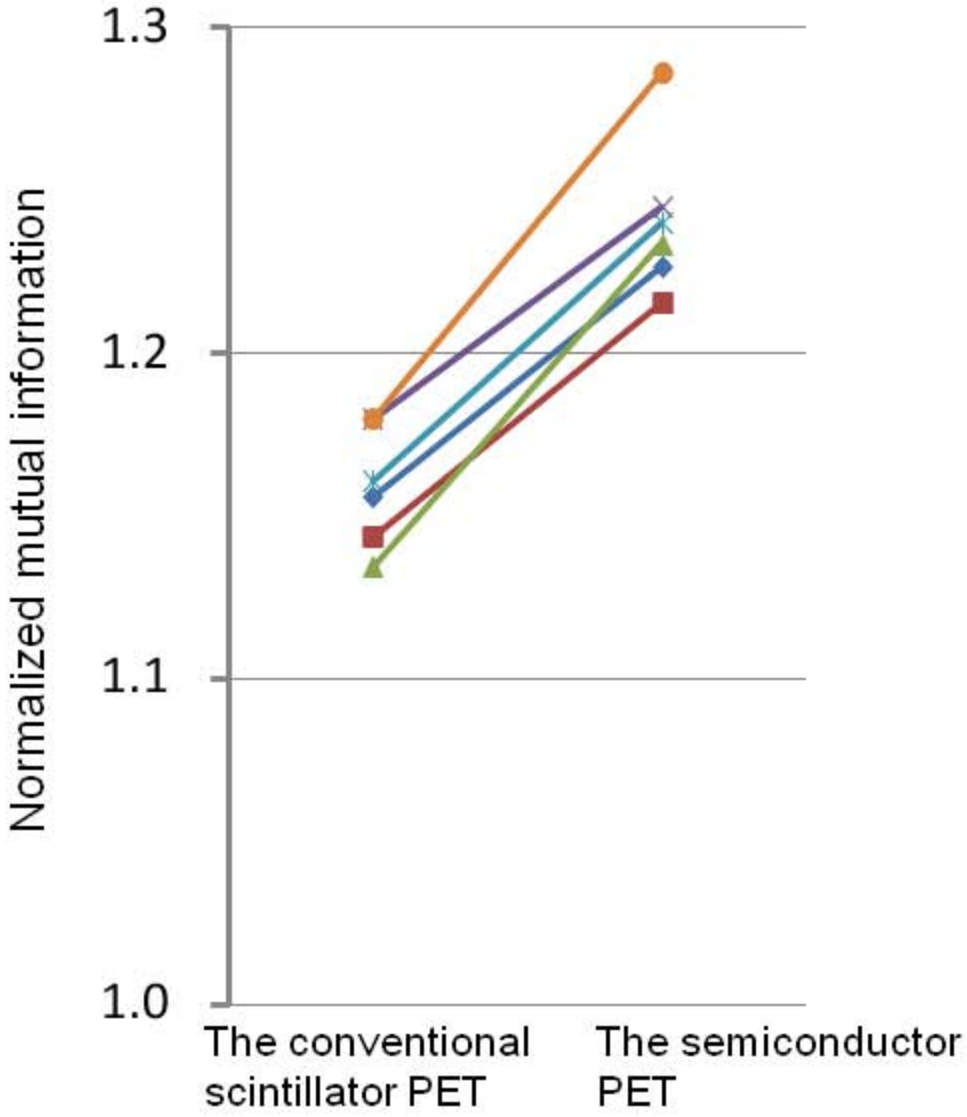
1.3
1.2
1.1
1.0
Normalized mutual information
The conventional scintillator PET
The semiconductor PET